2442–2456 *Nucleic Acids Research, 2020, Vol. 48, No. 5* *Published online 21 January 2020*
doi: 10.1093/nar/gkz1219

HSF2BP negatively regulates homologous recombination in DNA interstrand crosslink repair

Koichi Sato[1,†], Inger Brandsma[2,†], Sari E. van Rossum-Fikkert[2], Nicole Verkaik[2], Anneke B. Oostra[3], Josephine C. Dorsman[3], Dik C. van Gent[2], Puck Knipscheer[1,*], Roland Kanaar[2,*] and Alex N. Zelensky[2,*]

[1]Oncode Institute, Hubrecht Institute–KNAW and University Medical Center Utrecht, 3584 CT Utrecht, The Netherlands, [2]Department of Molecular Genetics, Oncode Institute, Erasmus University Medical Center, 3000 CA Rotterdam, The Netherlands and [3]Department of Clinical Genetics, VU University Medical Center, Van der Boechorststraat 7, 1081 BT Amsterdam, The Netherlands

Received August 7, 2019; Revised December 16, 2019; Editorial Decision December 18, 2019; Accepted December 20, 2019

ABSTRACT

The tumor suppressor BRCA2 is essential for homologous recombination (HR), replication fork stability and DNA interstrand crosslink (ICL) repair in vertebrates. We show that ectopic production of HSF2BP, a BRCA2-interacting protein required for meiotic HR during mouse spermatogenesis, in non-germline human cells acutely sensitize them to ICL-inducing agents (mitomycin C and cisplatin) and PARP inhibitors, resulting in a phenotype characteristic of cells from Fanconi anemia (FA) patients. We biochemically recapitulate the suppression of ICL repair and establish that excess HSF2BP compromises HR by triggering the removal of BRCA2 from the ICL site and thereby preventing the loading of RAD51. This establishes ectopic expression of a wild-type meiotic protein in the absence of any other protein-coding mutations as a new mechanism that can lead to an FA-like cellular phenotype. Naturally occurring elevated production of HSF2BP in tumors may be a source of cancer-promoting genomic instability and also a targetable vulnerability.

INTRODUCTION

BRCA2 is a large nuclear protein, mutations affecting it predispose to breast, ovarian and other forms of cancer (1). The tumor suppressor activity of BRCA2 is attributed to its functions in genome maintenance: error-free DNA double strand break (DSB) repair by homologous recombination (HR) and replication fork stabilization. These functions of BRCA2 depend on its association with other HR proteins: RAD51, PALB2 and BRCA1 (2), which also act as tumor suppressors. We recently characterized a novel direct interaction of BRCA2 with the protein HSF2BP (3), which is required for HR during meiosis (3,4). Physiological expression of *HSF2BP* is restricted to germline and ES cells (3–5), but we found that in some human tumors it is transcribed at high levels. This raises the question whether ectopic production of HSF2BP has a pathological effect on the function of BRCA2 in somatic cancer-derived cells.

The role of BRCA2 in HR is believed to be in delivering RAD51 to the sites of damage, and in performing the 'HR mediator' function: replacing the single-stranded DNA binding protein RPA with RAD51 (6). BRCA2 further stabilizes the resulting RAD51 nucleoprotein filament that then executes homology recognition and strand exchange reactions underlying most forms of HR. Therefore, BRCA2-deficient cells cannot faithfully repair DNA lesions that require HR. One example of such lesions are replication-associated DSBs that form when cells are treated with poly (ADP-ribose) polymerase inhibitors (PARPi), a new class of anticancer drugs (7). BRCA2 deficiency is synthetically lethal with PARPi, which makes these inhibitors promising chemotherapeutic agents for HR-deficient tumors.

Another type of DNA damage that stalls replication and results in replication-associated DSBs, which require HR for repair, are DNA interstrand crosslinks (ICLs) (8). These complex lesions arise from endogenous sources and are induced by clinically important chemotherapeutic drugs such as cisplatin and mitomycin C (MMC). ICL repair involves a large group of proteins, named FANCA to FANCW including BRCA2 (FANCD1), RAD51 (FANCR), PALB2 (FANCN) and BRCA1 (FANCS), known as the Fanconi anemia (FA) pathway. Defects in this pathway cause the hu-

*To whom correspondence should be addressed. Tel: +31 10 7043450; Fax: +31 10 7044743; Email: a.zelensky@erasmusmc.nl
Correspondence may also be addressed to Puck Knipscheer. Email: p.knipscheer@hubrecht.eu
Correspondence may also be addressed to Roland Kanaar. Email: r.kanaar@erasmusmc.nl
†The authors wish it to be known that, in their opinion, the first two authors should be regarded as joint First Authors.

man genetic cancer-predisposition syndrome FA (9). Cells from FA patients are acutely sensitive to ICL-inducing agents. Upon stalling of the replication machinery at the ICL, the FA pathway is activated via ubiquitination of the FANCD2-FANCI dimer by the FA core E3 ligase complex. Ubiquitinated FANCI-FANCD2 promotes nucleolytic disengagement of the crosslinked strands ('lesion unhooking') by the XPF-ERCC1 nuclease (10) resulting in the generation of a DSB, which can be repaired by HR (11). The replication fork protection function of BRCA2, associated with its C-terminal domain, likely also contributes to ICL repair, because deletion of this domain sensitizes mouse cells to ICL-inducing agents (12), and because in biochemical assays HR protein accumulation at the site of ICL precedes DSB formation (11).

Although germline mutations in *BRCA2* are responsible for only a small fraction of total breast cancer cases (<5%), many more tumors are functionally HR-deficient (e.g. ref. 13). This phenotypic resemblance ('BRCAness' (14)) is of high clinical significance, as it can guide the selection of treatment, in particular the use of PARPi and ICL-inducing compounds. Genetic analysis of HR-deficient cancers is focused on identifying mutations that affect protein-coding sequence (13). Similarly, known FA-causing mutations result in alteration of the protein coding sequence either directly or via splicing. Aberrant expression of a wild-type gene, such as what we reported for the meiotic HR gene *HSF2BP*, is generally not considered as a possible reason for HR disfunction in tumors or as an underlying cause of the FA. Since in most cases of tumors showing the BRCAness phenotype, as well as some cases of FA, the driver factors have not been identified, exploring such additional mechanisms can be clinically highly relevant.

Ectopic activation of the germline genes in cancer is ubiquitous and may be one of its hallmarks (15–18). Hundreds such genes have been identified, primarily as potential targets for anti-tumor immune therapy ('cancer/testis antigens' (CTA)) (15,19–20). For nearly all of them, the physiological function in the germline and the pathological role in cancer are unknown. The idea that ectopic expression is not epiphenomenal but contributes to cancer evolution and possibly even emergence is conceptually appealing (21,22), but remains largely untested. Given the central role genomic instability plays in tumorigenesis, many properties of meiotic DNA metabolism may be particularly relevant. However, only few out of hundreds of ectopically expressed germline-specific proteins have been shown to affect genome stability (21,23–30). Notably, two synaptonemal complex proteins were reported to affect mitotic HR, by either promoting (HORMAD1 (28,29)) or inhibiting it (SYCP3 (24) and also HORMAD1 (30)), although the mechanisms or relation to meiosis are not clear. Providing more detailed mechanistic understanding of such effects and connecting them to physiological roles would be extremely informative for both molecular oncology and reproductive biology fields.

In this report, we show that elevated ectopic production of HSF2BP in human cancer cells, through its interaction with BRCA2, disrupts HR in the context of ICL repair, phenocopying FA patient cells, and sensitizes cells to ICL-inducing agents and PARPi. The mechanism of ICL repair disruption by HSF2BP involves removal of BRCA2 from the ICL followed by proteasomal degradation. This reduces RAD51 accumulation at ICL damage site, thus inhibiting the HR step of the FA pathway of ICL repair. We demonstrate that the HSF2BP meiotic protein is a novel negative regulator of BRCA2 in somatic cells and propose that it could be exploited in cancer therapy.

MATERIALS AND METHODS

Cell culture

HeLa, U2OS, MDA-MB-157, HEK293T and RT-112 cells were cultured in DMEM, supplemented with 10% (v/v) fetal calf serum (FCS), 200 U/ml penicillin, 200 μg/ml streptomycin. HCC1187 were cultured in RPMI-1640 supplemented with 10% FCS, 200 U/ml penicillin, 200 μg/ml streptomycin and 0.25 μg/ml gentamycin.

Generation of genetically modified cell lines

With the exception of U2OS GFP-HSF2BP clone #5, all stable cell lines were constructed using PiggyBac vectors by co-transfecting them with the transposase expression construct (mPB (31) or hyPBase (32)), followed by selection with either 1.5 μg/ml puromycin or 800 μg/ml G418, depending on the construct, maintained for 6–10 days. Stable transformation was highly efficient (>95% GPF-positive cells when GFP-tagged constructs were used) and therefore clonal isolation was not performed. Stable line U2OS GFP-HSF2BP clone #5 used in the initial experiments (Figure 1A–C) was constructed by random integration of pEGPFN1-HSF2BP construct with 800 μg/ml G418 selection. Several GFP-positive individual clones were isolated, expanded and checked for uniform expression of single major GFP-fused protein by FACS and immunoblotting.

BRCA2$^{\Delta 12/\Delta 12}$ cell lines were produced by transfecting HeLa cells with sgRNA cloned into pX459 Cas9 expression vector (33). Target sequences for sgRNAs in introns 11 and 12 were CTATTTAACAGGGTCTAAAC and AGTGACAATACTTATTGCCG, respectively. Cells were cloned by limiting dilution and screened by PCR for the loss or inversion of the targeted region (primers F1: TTGTTA GGCCTTATTGCCAGT, R: AGCTAATTTTACCATC TGGAGTGC and R3: CCTTTTACTTGAAAGAATAA CCAAC). Positive clones were expanded, and loss of wild-type transcript was verified by RT-PCR with primers A: CA CCTACGTCTAGACAAAATGTATC, B: GTGCCATC TGGAGTGCTTTT, C: GCCTGGCTGTGGAAAGAC GCGTTGCCTTTG and D: GGCATCTATTAGCAAA TTCCTTAGGAAAGGCACATTCCAT.

Expression constructs

Cloning of human and mouse HSF2BP from U2OS and mES IB10 cells and engineering of GFP-HSF2BP expression constructs was described previously (3). Untagged HSF2BP expression constructs were produced similarly, in the same PiggyBac vectors (34) using PCR amplification and Gibson assembly (35). Details of the PCR primers and cloning strategies are available upon request.

Lentiviral shRNA transduction

shRNA expression constructs were obtained from the Sigma mission library (TRC 1.5). Lentiviral packaging plasmids (pMDLg/pRRE, pRSV-REV and pMD2.G) and shRNA expression constructs were transfected into HEK293T cells using calcium phosphate precipitation: HEK293T cells were seeded at a density of 12–20 $\times$ 10^6 per 10-cm culture dish in 17 ml media; transfection was performed within 1–6 h after seeding: 30 μg DNA (12 μg lentiviral genome and 6 μg of each of the packaging plasmid) was dissolved in 900 μl deionized water and mixed with 100 μl 2.5 M $CaCl_2$, 1 ml of 2 $\times$ HBS buffer (50 mM HEPES, 280 mM NaCl, 1.5 mM Na_2HPO_4, pH 7.1 with NaOH, filter-sterilized) was added dropwise, while air bubbles were passed through the DNA solution to ensure mixing. Transfection mix was added to the plates containing HEK293T cells dropwise within 5–10 min after mixing; 24 h after transfection the medium was changed and 48 h after transfection the supernatant of the HEK293T cells was added to U2OS cells. This process was repeated the next day. Forty-eight hours after the second transduction, selection with 1.5 μg/ml puromycin was started. Two of the five tested shRNAs efficiently reduced the concentration of overproduced GFP-HSF2BP: #2 (clone TRCN0000017473, target sequence GCTGGA ATTGTCACGAATGTT) and #3 (clone TRCN00000174 76, target sequence GCTAATGCTGATGTCCCTATA); constructs SHC001 (empty vector) and SHC003 (non-targeting shRNA) from the same library were used as negative controls.

Clonogenic survivals

Clonogenic survivals were performed in 6-well plates with technical duplicates or triplicates and done at least twice. Cells maintained in 6-well plates before the start of experiment were trypsinized and counted either manually, using Z2 counter (Beckman Coulter) or using Countess II counter (Thermo). The basal seeding density of 100 cells per untreated well was adjusted in dose-dependent manner to account for plating efficiency reduction due to treatment. Olaparib (AstraZeneca, AZD2281) and talazoparib (BMN 674, Axon Medchem) were added to the media on the day of seeding after cells became attached. Media was replaced 4 days after olaparib addition. MMC treatment was performed one day after seeding; after 2 h incubation with MMC, media were removed, cells were rinsed with PBS and 2 ml fresh media were added. After 6–8 days plates were rinsed with PBS, stained with Coomassie brilliant blue R (0.025% in 40% methanol, 10% acetic acid), and macroscopically visible colonies were counted manually or using the OpenCFU software (36). In the figure legends, *n* indicates the number of biological replicates, error bars indicate s.e.m. between means of technical replicates in each experiment where $n \geq 3$, or between all individual technical replicates in experiments with $n = 2$. For genetically engineered *BRCA2* Δ12 cells, three independent clones were used per genotype and considered as biological replicates when calculating the mean.

DR-GFP assay

U2OS cells carrying the reporter (clone U2OS-18 (37)) were transfected with the PiggyBac expression construct for HSF2BP or empty vector, and the construct encoding transposase, stable integrants were selected with 800 μg/ml G418. The stably transformed U2OS-18 derivatives were seeded into 6-well plates at 2 $\times$ 10^5 cells per well and transfected next day using XtremeGene reagent with 2 μg of either I-SceI expression plasmid (pCBASceI), empty vector or pEGFP-N1 as transfection control efficiency control. FACS analysis was performed 2 days after transfection as previously described (38) but a BD LSRFortessa cell analyzer was used.

Antibodies

Antibodies used in this study were against RAD51 (rabbit 2307 (39)), FANCD2 (NB 100-316, Novus Biologicals), H2B (07-371, Millipore), MSH2 (Ab-2, Oncogene), HSP90 (ab13492, Abcam), BRCA2 (Ab-1, OP95, Calbiochem), GFP (clones 7.1 and 13.1, Roche), PARP-1 (C2-10, Enzo), 6xHis tag (ab18184, Abcam), Actin (clone C4, MAB1501, Millipore) and ubiquitin (sc-8017, Santa Cruz Biotechnology). Anti-HSF2BP rabbit polyclonal antibodies SY8126 and SY8127 were raised against purified recombinant untagged human HSF2BP (Kaneka Eurogentec, Belgium) and used either as crude serum or after affinity purification against GST-HSF2BP immobilized on glutathione sepharose as described (40). Antibodies against *Xenopus laevis* (xl) REV1, xlXPF,xlERCC1, xlBRCA2, xlPCNA and xlFANCD2 were previously described (3,10,41–44).

Immunoblotting and cell fractionation

To prepare total protein lysates, cells were scraped in PBS or collected by trypsinization and lysed in 2× Laemmli SDS loading buffer (120 mM Tris pH 6.8, 4% SDS, 10% glycerol), after determining the protein concentration in the lysate by Lowry method, the lysate was complemented with 10× reducing additive (0.1% bromophenol blue, 0.5% β-mercaptoethanol). For fractionation (45), 1 million cells were collected by trypsinization, washed with ice-cold PBS, re-suspended in Schaffner's lysis buffer (10 mM HEPES-NaOH pH 7.9, 10 mM KCl, 0.1 mM EDTA, 0.1 mM EGTA, 1 mM dithiothreitol (DTT), protease inhibitor cocktail); after 15-min incubation on ice NP-40 was added to the final concentration 0.1% and solution was vortexed. Nuclei were pelleted by 30 s centrifugation at 18 000 rcf, re-suspended by shaking for 15 min at 4°C in nuclear extraction buffer (20 mM HEPES-NaOH pH 7.9, 400 mM KCl, 1 mM EDTA, 1 mM EGTA, 1 mM DTT, protease inhibitor cocktail) and centrifuged for 5 min at 18 000 rcf to separate chromatin pellet from soluble nucleoplasmic fraction; the pellet was re-suspended in Laemmli SDS loading buffer. Proteins were separated on polyacrylamide hand-cast tris-glycine or bis-tris, or precast bis-tris or tris-acetate gels (Novex) and blotted on nitrocellulose or PVDF membranes. For hHSF2BP immunodetection with SY8126 antibody in whole cell extracts, hand-cast bis-tris gels were used (14% acrylamide/bis 37.5; 3.5× Bis-Tris gel buffer

(1.25 M Bis-Tris HCl, pH 6.6) diluted to 1× with water) and run with the MES-SDS running buffer (ThermoFisher, NP0002) at 100 V for 5 h. For BRCA2 detection 4–8% precast tris-acetate gels were used, and transfer was performed in 2× Towbin transfer buffer (50 mM Tris, 384 mM glycine, 20% methanol) at 300 mA constant current for 2 h at 4°C to PVDF membrane. Membranes were blocked in 5% milk in PBS supplemented with 0.05% Tween. After overnight incubation with the primary antibody, membranes were washed in PBS supplemented with 0.05% Tween and incubated with horseradish peroxidase-conjugated secondary antibodies (Jackson Immunoreserach). Blots were developed using homemade ECL reagents and detected with the Alliance 4.7 (UVItec) or Amersham Imager 600 (GE Healthcare).

Protein purification

Human HSF2BP, human HSF2BP variant R200T and *Xenopus laevis* HSF2BP were purified as previously described (3). For the purification of FLAG-His tagged ubiquitin, the cDNA encoding *Xenopus laevis* ubiquitin was ligated into pETDuet-1 vector. The ubiquitin protein was overexpressed with a N-terminal FLAG-His tag in *E. coli* BL21(DE3) cells at 30°C and purified with Ni-NTA agarose resin by the same method as *Xenopus laevis* HSF2BP. Eluted protein was dialyzed against 2 mM β-mercaptoethanol (4 l) overnight and then applied to 30 kDa MWCO Amicon Ultra-15 centrifugal filter unit (Millipore). After centrifugation, flow-through was collected, concentrated using 3 kDa MWCO Amicon Ultra-15 centrifugal filter unit (Millipore) and flash frozen with liquid nitrogen. The concentration of the proteins was determined by SDS-PAGE with Coomassie Brilliant Blue staining, using BSA as the standard protein.

Xenopus egg extracts, immunodepletion, DNA replication, repair assay and lesion bypass assay

DNA replication and preparation of *Xenopus* egg extracts (HSS and NPE) were performed as described previously (46,47). Preparation of plasmid with a site-specific cisplatin ICL (pICL) and ICL repair assays was performed as described (43,48). Briefly, pICL (9 ng/μl) and pQuant (0.45 ng/μl) were first incubated in a high-speed supernatant (HSS) of egg cytoplasm for 20 min at ∼20°C, which promotes the assembly of prereplication complexes on the DNA. Addition of two volumes nucleoplasmic egg extract (NPE), which also contained ^{32}P-α-dCTP, triggers a single round of DNA replication. Where indicated, His-tagged human HSF2BP (0.45 μM) or His-tagged *Xenopus laevis* HSF2BP (0.45 μM), FLAG-His tagged ubiquitin (0.11 μg/μl), MG-132 (0.38 mM) or NMS-873 (0.2 mM) was added to NPE prior to mixing with HSS. Aliquots of replication reaction (3.8 μl) were stopped at various times with 45 μl Stop solution II (50 mM Tris pH 7.5, 0.5% SDS and 10 mM EDTA,). Samples were incubated with RNase (0.13 μg/μl) for 30 min at 37°C followed by proteinase K (0.5 μg/μl) overnight at room temperature. DNA was extracted using phenol/chloroform, ethanol-precipitated in the presence of glycogen (30 mg/ml) and resuspended in 3.8 μl TE (10 mM Tris pH 7.5 and 1 mM EDTA). ICL repair was analyzed by digesting 1 μl extracted DNA with HincII, or HincII and SapI, separation on a 0.8% agarose gel in 1× TBE buffer, and quantification using Typhoon TRIO+ (GE Healthcare) and ImageQuant TL software (GE Healthcare). Repair efficiency was calculated as described (49). For lesion bypass assay, the digested DNA was ethanol-precipitated, and resuspended in 12 μl alkaline loading buffer (50 mM NaOH, 1 mM EDTA and 2.5% Ficoll-400). Fragments were then separated on a 0.8% agarose gel in alkaline buffer (50 mM NaOH and 1 mM EDTA), after which the gel was dried on Amersham Hybond-XL membrane (GE Healthcare) and exposed to a phosphor screen. The band intensity of the bypassed product was quantified with Typhoon TRIO+ using ImageQuant TL software (GE Healthcare). The highest value was set at 100% for the bypassed product. Immunodepletion of the XPF-ERCC1 complex was performed using Protein A Sepharose Fast Flow (PAS) beads (GE Healthcare) as previously described (10).

Immunofluorescence and microscopy

HeLa cells were treated overnight with 100 nM or for 2–4 h with 1.2 μM MMC, washed with PBS, pre-extracted before fixation for 1 min in Triton X-100 buffer (0.5% Triton X-100, 20 mM HEPES-KOH pH 7.9, 50 mM NaCl, 3 mM $MgCl_2$, 300 mM sucrose), fixed in 2% paraformaldehyde in PBS and stained as described (50). In short-term treatment experiments, EdU was added to final concentration 10 μM 30 min before pre-extraction and fixation. Cells were then permeabilized with 0.5% Triton in PBS, washed with 3% BSA in PBS; Atto-594 azide (Atto Tec, #594–105, final concentration 60 μM) conjugation reaction was performed in 50 mM Tris pH 7.5, 4 mM $CuSO_4$, 10 mM ascorbic acid, followed by RAD51 immunofluorescence staining. Pictures were taken using a Leica SP5 confocal microscope using a 63× objective and 405, 488 and 594 nm lasers. Statistical analysis was performed in Graphpad Prism using a Kruskal–Wallis test with Dunn's post-test.

Incision assay

Incision assay was performed as described previously (10,51). Briefly, pICL (225 ng) and pQuant (11.3 ng) were incubated with 1.5 units NB-BSR DI enzyme (NEB) in 1× NEBuffer 2.1 for 30 min at room temperature. Subsequently, the nick translation reaction was initiated by adding 11 μl DNA Polymerase I mix (5 units DNA polymerase I (NEB), dATP, dGTP, dTTP (0.5 mM each), dCTP (0.4 μM) and ^{32}P-α-dCTP (3.3 μM) in 1 × NEBuffer 2.1) and incubation for 3 min at 16°C. The reaction was stopped with 180 μl Stop Solution II, treated with proteinase K (0.24 mg/ml) and phenol/chloroform-extracted. After excess label was removed using a Micro Bio-Spin 6 Column (Bio-Rad), plasmids were ethanol-precipitated, and resuspended in 5 μl ELB (10 mM HEPES-NaOH pH 7.7, 50 mM KCl, 2.5 mM $MgCl_2$ and 250 mM Sucrose). The labeled plasmid was used in a replication reaction and samples at various times were extracted and digested with HincII. Fragments were separated on a 0.8% denaturing agarose gel in alkaline

buffer, after which the gel was dried on Amersham Hybond-XL membrane and exposed to a phosphor screen. The band intensity of the X-shape structure was measured with Typhoon TRIO+ and quantified using ImageQuant TL software. The highest value was set at 100% for the X-shape structure.

Two-dimensional gel electrophoresis (2DGE)

2DGE was performed as described previously (11). Replication samples of pICL at various times were extracted and digested with HincII. Fragments were then analyzed by 2DGE. The first dimension gel consisted of 0.4% agarose run in 0.5× TBE buffer at 0.86 V/cm for 24 h at room temperature. The lanes of interest were cut out, casted across the top of the second-dimension gel consisting of 1% agarose with 0.3 μg/ml ethidium bromide, and run in 0.5× TBE containing 0.3 μg/ml ethidium bromide with buffer circulation at 3.5 V/cm for 14.5 h at room temperature. The gel was dried on Amersham Hybond-XL membrane and exposed to a phosphor screen. DNA was visualized using a Typhoon TRIO+.

Plasmid pull-down assay

Plasmid pull-down assay was performed as described previously with modifications (41). At the indicated times, 5 μl of the pICL replication samples were mixed with 3.75 μl LacI-coupled magnetic beads (Dynabeads M-280; Life Technologies) suspended in 25 μl ELB containing 0.25 mg/ml BSA, 2.5 mM $CaCl_2$ and 0.03% Tween 20, and incubated for 30 min on ice. The beads were washed three times with 37.5 μl ELB containing 0.25 mg/ml BSA, 2.5 mM $CaCl_2$ and 0.02% Tween 20, dried, and suspended in 20 μl 1× SDS sample buffer. Plasmid-bound proteins were then separated by SDS-PAGE and visualized by western blotting using the indicated antibodies.

Chromatin immunoprecipitation (ChIP)

ChIP was performed as described previously (52). At the indicated times, pICL replication samples were crosslinked with ELB containing 1% formaldehyde for 10 min at room temperature. A non-related undamaged control plasmid (pQuant) was added to the replication reactions to assess background binding of the proteins. After quenching the formaldehyde by addition of glycine (125 mM final concentration), the samples were passed through a Micro Bio-Spin 6 Chromatography column (Bio-Rad), sonicated and immunoprecipitated with 5 μg of the indicated antibodies bound to PAS beads. The protein-bound DNA fragments were eluted with ChIP elution buffer (50 mM Tris pH 7.5, 10 mM EDTA and 1% SDS) and the crosslinks were reversed by incubation at 42°C for 6 h and subsequently at 70°C for 9 h. DNA was then phenol/chloroform-extracted, followed by quantitative real-time PCR in 10 μl reaction buffer (6 mM Tris pH 8.3, 25 mM KCl, 2.5 mM $MgCl_2$, 0.1% Tween-20, 0.1 mg/ml BSA, 0.3 mM dNTPs, 1:66,500 SYBR Green I (Sigma-Aldrich), and Hot Start Taq DNA polymerase), using 0.25 μM of following primers: pICL (5′-AGCCAG ATTTTTCCTCCTCTC-3′ and 5′-CATGCATTGGTTCT GCACTT-3′) and pQuant (5′-TACAAATGTACGGCCA GCAA-3′ and 5′-GAGTATGAGGGAAGCGGTGA-3′). The values from pQuant primers were subtracted from the values for pICL primers. Antibodies used for ChIP were purified with PAS beads.

RESULTS

HSF2BP causes DNA damage sensitivity in somatic cells

We previously reported that transcripts encoding HSF2BP, despite being restricted to the germline in mice, are detected in all human cancer cell lines we tested, and that in some tumor samples their levels approach those observed in normal testis (3). Analysis on the total protein extracts from several cell lines by anti-HSF2BP immunoblotting (Supplementary Figure S1A) was consistent with this varying degree of expression and the presence of alternatively spliced forms we described previously (3). This indicates that either the *HSF2BP* promoter can be activated or the gene can be amplified, in cancer cells of non-testicular origin. To test the effect of ectopic activation of *HSF2BP*, we performed RNAi and overproduction experiments in HeLa and U2OS cells in which HSF2BP protein is hardly detectable (Figure 1A and Supplementary Figure S1B), despite the presence of the transcript (3). While knockdown of HSF2BP did not affect clonogenic survival of U2OS cells, increasing its ectopic production by stably expressing GFP-tagged *HSF2BP (GFP-HSF2BP)* led to hypersensitization to ICL-inducing agent MMC (Figure 1B). The effect was reverted by RNAi against HSF2BP, confirming the specificity (Figure 1B). We further established that elevated production of untagged human or murine HSF2BP (hHSF2BP and mHSF2BP, respectively) in Hela induced sensitivity to MMC, cisplatin and the PARP inhibitor olaparib, while not affecting cell viability (Supplementary Figure S1B–F). Importantly, overproduction of HSF2BP did not sensitize Hela or U2OS cells to ionizing radiation (Figure 1C, and Supplementary Figure S1G), which indicates that HSF2BP affects some, but not all, functions of BRCA2.

Genomic instability induced by HSF2BP could be beneficial for tumor evolution, and mutations increasing its production could be positively selected in tumors. To investigate this, we searched for alterations in *HSF2BP* gene copy number using the cBioPortal Cancer Genomics database (53,54), and found that it is frequently amplified, reaching 1–2% in breast and ovarian cancers (Figure 1D). Moreover, amplification of *HSF2BP* rarely overlapped with mutations in *BRCA2*, indicating that these events are likely mutually exclusive (Figure 1E). This indicates that elevated levels of HSF2BP, through its previously reported interaction with BRCA2 (3), could play a role in cancer development.

HSF2BP inhibits the FA pathway

Hypersensitivity to DNA crosslinking agents and PARP inhibitors in the absence of ionizing radiation sensitivity or proliferation defects is more similar to the phenotype of patient cells deficient in the FA proteins, rather than in general HR components. Consistent with this, we found no effect on DSB-induced direct repeat GFP gene conver-

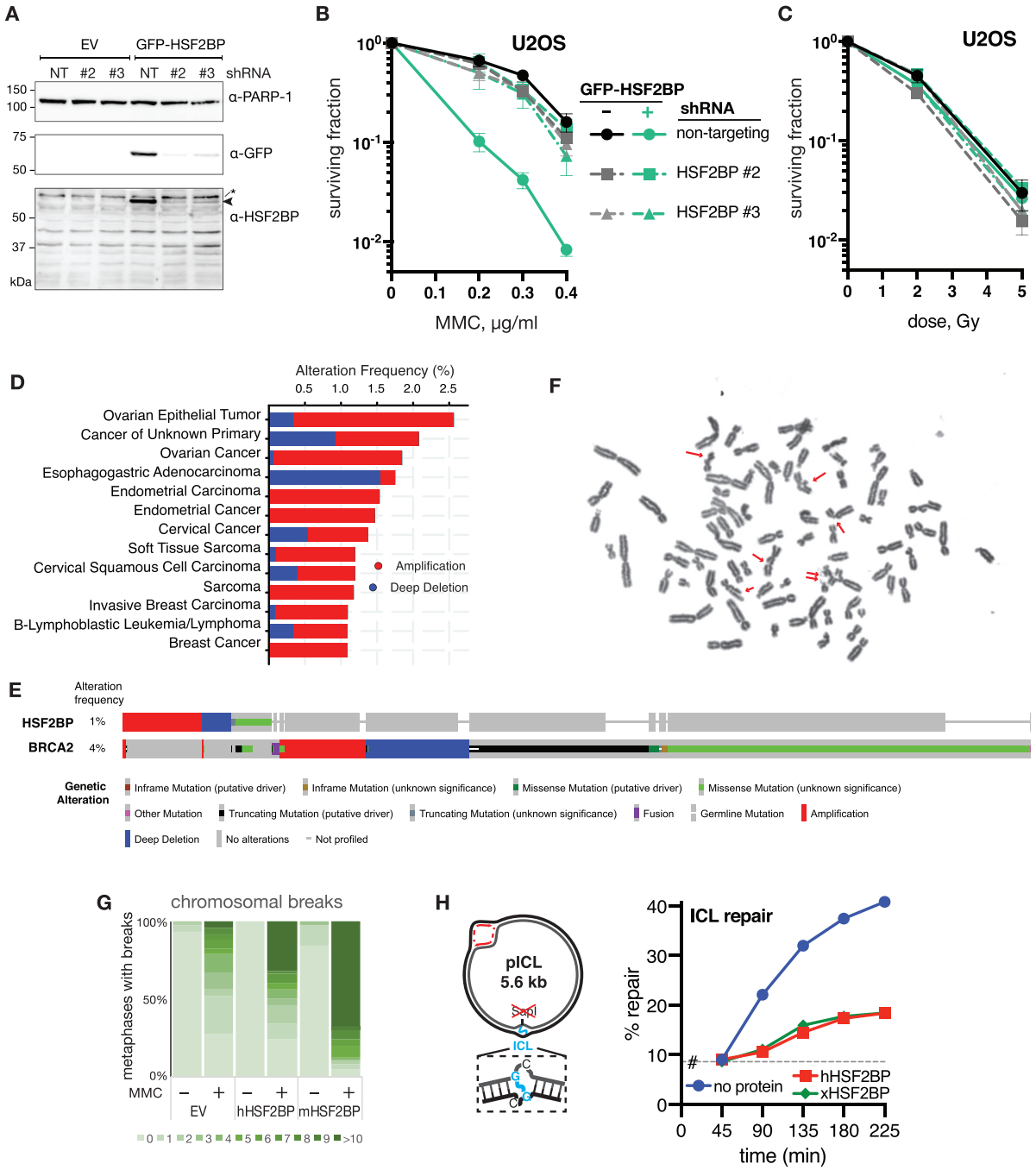

Figure 1. HSF2BP disrupts the FA pathway. (**A–C**) Immunoblot and clonogenic survivals of the U2OS cells stably transformed with GFP-hHSF2BP or GFP expression constructs and stably transduced with lentiviral vectors encoding anti-HSF2BP (#2, #3) or non-targeting shRNAs. Cells were treated with the indicated doses of MMC (B) or ionizing radiation (C); $n = 2$. Efficiency of the knockdown was assessed by immunoblotting of whole cell extracts with the indicated antibodies (A); * indicates a non-specific band. (**D**) Frequency of *HSF2BP* deletion and amplification in tumor sample sequencing data available at cBioPortal (53,54). Studies with ≥100 samples were analyzed. (**E**) Graphical summary of cancer samples that harbor genetic alteration in either the *HSF2BP* or *BRCA2* gene. Alteration frequency was calculated using profiled samples (562 alterations in 55 817 profiled samples for *HSF2BP*, and 2945 alterations in 68 793 profiled samples for *BRCA2*). Each sample was colored by alteration types as indicated. (**F**) Example metaphase chromosomal spread from HSF2BP-overproducing cell treated overnight with 100 nM MMC. Chromatid breaks and a quadriradial chromosome are indicated with single and double arrows, respectively. (**G**) Quantification of chromatid breaks in HeLa cells stably transformed with HSF2BP expression vectors or control, with and without overnight 100 nM MMC treatment; 50 metaphases per condition were scored. (**H**) ICL repair efficiency in the presence or absence of HSF2BP. The scheme on the left shows pICL, a synthetic plasmid substrate in which the diagnostic SapI site is disrupted by a cis-platinum ICL that is restored by replication-associated repair by the FA pathway in *Xenopus* egg extracts (see also (Supplementary Figure S3A) for details). pICL was replicated in *Xenopus* egg extract that was supplemented with purified recombinant His-tagged human (h) or Xenopus (x) HSF2BP or buffer. Replication intermediates were isolated and digested with HincII, or HincII and SapI, and separated on agarose gel. Repair efficiency was calculated and plotted. As repair kinetics and absolute efficiency are highly dependent on the egg extract preparation, single experiment is plotted here, and a replica is shown in (Supplementary Figure S1L). #, SapI fragments from contaminating uncrosslinked plasmid present in varying amounts in different pICL preparations.

sion in HSF2BP-overproducing cells (Supplementary Figure S1H), indicating that HR at restriction enzyme-induced DSBs was functional. Furthermore, HSF2BP induced a drastic increase in chromosomal aberrations, including radial chromosome formation, after treatment with MMC, another hallmark of FA patient cells (Figure 1F and G). These data suggest that ectopic production of HSF2BP specifically affects the role of BRCA2 in ICL repair by the FA pathway. Consistent with the specific effect, we found that BRCA2 concentration was not changed (Supplementary Figure S1I), and nuclear localization of BRCA2 was not affected (Supplementary Figure S1J) by HSF2BP overproduction.

To examine whether HSF2BP directly acts in the FA pathway of ICL repair, we took advantage of the evolutionary conservation of the HSF2BP–BRCA2 interaction (3) and made use of the *Xenopus* egg extract-based ICL repair system. This system fully recapitulates the repair of a single, site-specific cisplatin ICL situated on a plasmid, in a DNA replication- and FA pathway-dependent manner (43,49,55). We replicated the ICL-containing plasmid (pICL) in *Xenopus* egg extract, which does not contain detectable endogenous *Xenopus laevis* HSF2BP, in the presence or absence of recombinant HSF2BP. Replication intermediates were isolated and repair efficiency was determined by measuring the regeneration of a SapI recognition site that is blocked by the ICL prior to repair (Figure 1H). Addition of recombinant human or *Xenopus* HSF2BP reduced ICL repair efficiency by 70–80% (Figure 1H; Supplementary Figure S1K and L). These data strongly suggest that the sensitivity of cells ectopically producing HSF2BP to ICL-inducing agents is due to the inhibition of ICL repair by the FA pathway.

HSF2BP–BRCA2 interaction mediates FA pathway inhibition

Next, we examined whether direct interaction between HSF2BP and BRCA2 is required for ICL repair inhibition by disrupting the interactions sites of both proteins. In sharp contrast to wild-type HSF2BP, addition of the R200T mutant, which does not interact with BRCA2 as we previously showed (3), did not reduce ICL repair efficiency in *Xenopus* egg extract (Figure 2A and Supplementary Figure S2A). Consistent with this, the production of HSF2BP R200T did not sensitize U2OS cells to MMC (Figure 2B). In previous work, we reported that most of the HSF2BP-interacting region is encoded by exon 12 of the BRCA2 gene (3). To disrupt this region, we took advantage of a naturally occurring minor splice form of the BRCA2 transcript (56–59), in which exon 12 is skipped but the reading frame is preserved. We predicted that this $BRCA2^{\Delta 12/\Delta 12}$ isoform would be resistant to the inhibitory effect of HSF2BP and engineered variant HeLa cell lines, in which we excised exon 12 from both alleles of the *BRCA2* gene by CRISPR/Cas9 (Figure 2C and Supplementary Figure S2B). As we predicted, the $BRCA2^{\Delta 12/\Delta 12}$ cells were not sensitized to ICL-inducing agents and PARP inhibition upon ectopic HSF2BP expression, while $BRCA2^{wt}$ cells were (Figure 2D–G). Importantly, $BRCA2^{\Delta 12/\Delta 12}$ cells were not hypersensitive to ICL-inducing agents in absence of ectopic HSF2BP expression (Figure 2E and F). Thus, HSF2BP inhibition of ICL repair requires direct interaction with BRCA2.

HSF2BP inhibits homologous recombination in the FA pathway

BRCA2 could act at various stages of ICL repair; it has been assumed to play a role during HR, but it could also act further upstream in the response to stalled replication fork. To investigate which repair step is affected by HSF2BP addition, we made use of the synchronous ICL repair reaction in *Xenopus* egg extract (Supplementary Figure S3A). Early key events in cisplatin ICL repair by the FA pathway are FANCD2 monoubiquitination and the subsequent nucleolytic incisions (10,60). Incubation of pICL in *Xenopus* egg extract caused robust FANCD2 ubiquitination and this was not affected by addition of hHSF2BP (Figure 3A). Consistently, ectopic production of HSF2BP in human cells also did not affect FANCD2 ubiquitination (Supplementary Figure S3B). We next investigated if ICL unhooking was affected by HSF2BP. Unhooking incisions can be directly observed during ICL repair in egg extract by separating linearized replication intermediates on denaturing agarose gels (Figure 3B and Supplementary Figure S3C). The labeled parental strand migrates as a large X-shaped structure and upon ICL unhooking it is converted to a linear molecule and arms (10,55). We replicated prelabeled pICL in the presence and absence of hHSF2BP and measured the decline of the X-shape structures in time. However, no difference was observed in the presence or absence of hHSF2BP indicating that ICL unhooking was not affected by HSF2BP (Figure 3C).

After ICL unhooking, translesion synthesis (TLS) is initiated by the insertion of a nucleotide across from the unhooked adduct by a currently unknown polymerase, followed by strand extension mediated by REV1 and polymerase ζ (Supplementary Figure S3A) (41,43). TLS can be monitored by separating nascently labeled and linearized pICL replication products on a denaturing agarose gel. Stalled replication forks at the ICL initially generate arm fragments and these are then converted to fully extended linear fragments by TLS (Supplementary Figure S3A). Subsequently, the incised strand will be repaired by HR resulting in the accumulation of additional full-length linear fragments that are cleavable by SapI. Of note, the TLS products are not cleavable by SapI because the unhooked adduct is not removed in *Xenopus* egg extract (43). We separated HincII-digested nascent labeled repair products, which were replicated in the presence and absence of hHSF2BP, on a denaturing agarose gel and quantified the accumulation of linear products (Figure 3D and Supplementary Figure S3D). While linear products accumulated in both conditions, the increase was less in the presence of HSF2BP (Figure 3E). This could be caused by a defect in TLS and/or a defect in HR. To address this, we examined the repair intermediates after digestion with both HincII and SapI and found that the accumulation of full-length linear products was very similar in absence or presence of HSF2BP (Figure 3E). This shows that TLS is not affected by the addition of HSF2BP, and suggests that the reduction of linear products is caused by a defect in HR. To address this directly, repair interme-

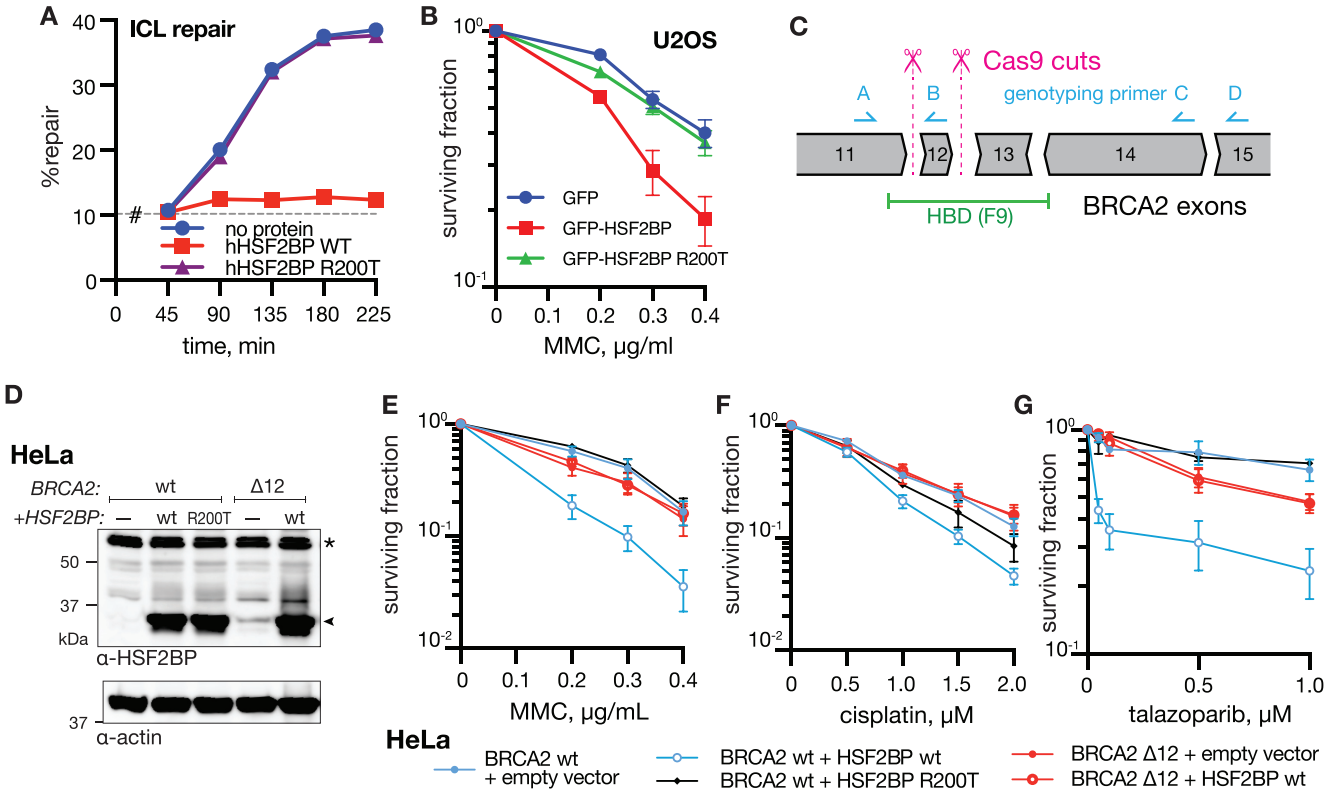

Figure 2. FA pathway disruption by HSF2BP requires interaction with BRCA2. (**A**) ICL repair efficiency in *Xenopus* egg extract in the presence or absence of purified recombinant wild-type (WT) human HSF2BP or its R200T variant that cannot bind BRCA2. #, SapI fragments from contaminating uncrosslinked plasmid present in varying amounts in different pICL preparations. Repeat of this experiment is shown in (Supplementary Figure S2A). (**B**) Clonogenic survival of U2OS cells stably producing GFP, or GFP-tagged wild-type or non-BRCA2-binding R200T variant of HSF2BP, and exposed to the indicated doses of MMC; $n = 4$. (**C**) Schematic of a fragment of the human *BRCA2* locus depicting the strategy for homozygous exon 12 excision from HeLa cells using two CRISPR/Cas9 cuts. Introns are not drawn to scale; exon phase is depicted using various shapes of the side boundaries. Genotyping primers are shown as blue arrows (see also (Supplementary Figure S2B)). Boundaries of the minimal HSF2BP-binding domain (HBD) mapped in the previous study (fragment F9 (3)) is shown with green line. (**D–G**) Immunoblot (D) and clonogenic survival (E and F) of the *BRCA2 Δ12* and its parental HeLa cell line (wt), stably transformed with human HSF2BP expression vector (wild-type or R200T mutant) or empty vector. (D) HSF2BP is indicated with an arrow, * – non-specific band. For clonogenic survivals cells were treated with ICL-inducing agents MMC (E) and cisplatin (F), or PARPi talazoparib (G); $n = 3–9$.

diates were linearized and analyzed by 2D gel electrophoresis (Figure 3F). In the absence of hHSF2BP, an X-arc was formed indicating the presence of HR intermediates (11). In contrast, the presence of wild-type hHSF2BP, but not the R200T mutant, inhibited the formation of the X-arc (Figure 3G and Supplementary Figure S3E), providing further evidence that HR during ICL repair is affected by HSF2BP.

HSF2BP reduces loading of RAD51 to ICLs

To address how HSF2BP inhibits HR during ICL repair, we investigated BRCA2 and RAD51 recruitment to the ICL-containing DNA. To this end, we pulled down the crosslinked plasmid DNA during ICL repair in *Xenopus* egg extract using streptavidin beads coated with biotinylated LacI protein, which binds efficiently and nonspecifically to DNA (41) (Figure 4A). While this assay was not sensitive enough to detect BRCA2, RAD51 was readily accumulated on pICL in the absence of hHSF2BP (Figure 4B). In contrast, no RAD51 was detected on pull downs in the presence of hHSF2BP (Figure 4B). Consistent with this, RAD51 accumulation at sites of MMC-induced damage in human cells was significantly reduced by HSF2BP (Figure 4C and D; Supplementary Figure S4A). To investigate the binding of BRCA2 specifically to the ICL site, we then employed chromatin immunoprecipitations (ChIP; Figure 4E). BRCA2 was immunoprecipitated from ICL repair reactions in the presence and absence of HSF2BP, and the co-precipitated DNA was amplified by quantitative PCR with primers specific to the ICL region. BRCA2 accumulated at the ICL during repair as previously described (61). However, in the presence of HSF2BP, the accumulation of BRCA2 at the site of damage was not only reduced, but also more transient as BRCA2 levels returned to background faster compared to conditions in which no HSF2BP, or HSF2BP R200T were added (Figure 4F). HSF2BP itself was recruited to the ICL in a BRCA2-dependent manner as its wild-type form co-immunoprecipitated with the pICL, while the R200T mutant did not (Figure 4G), which is consistent with the defective HSF2BP DNA-damaged induced focus formation observed for this mutant (3). In contrast, recruitment of the unhooking endonuclease XPF,

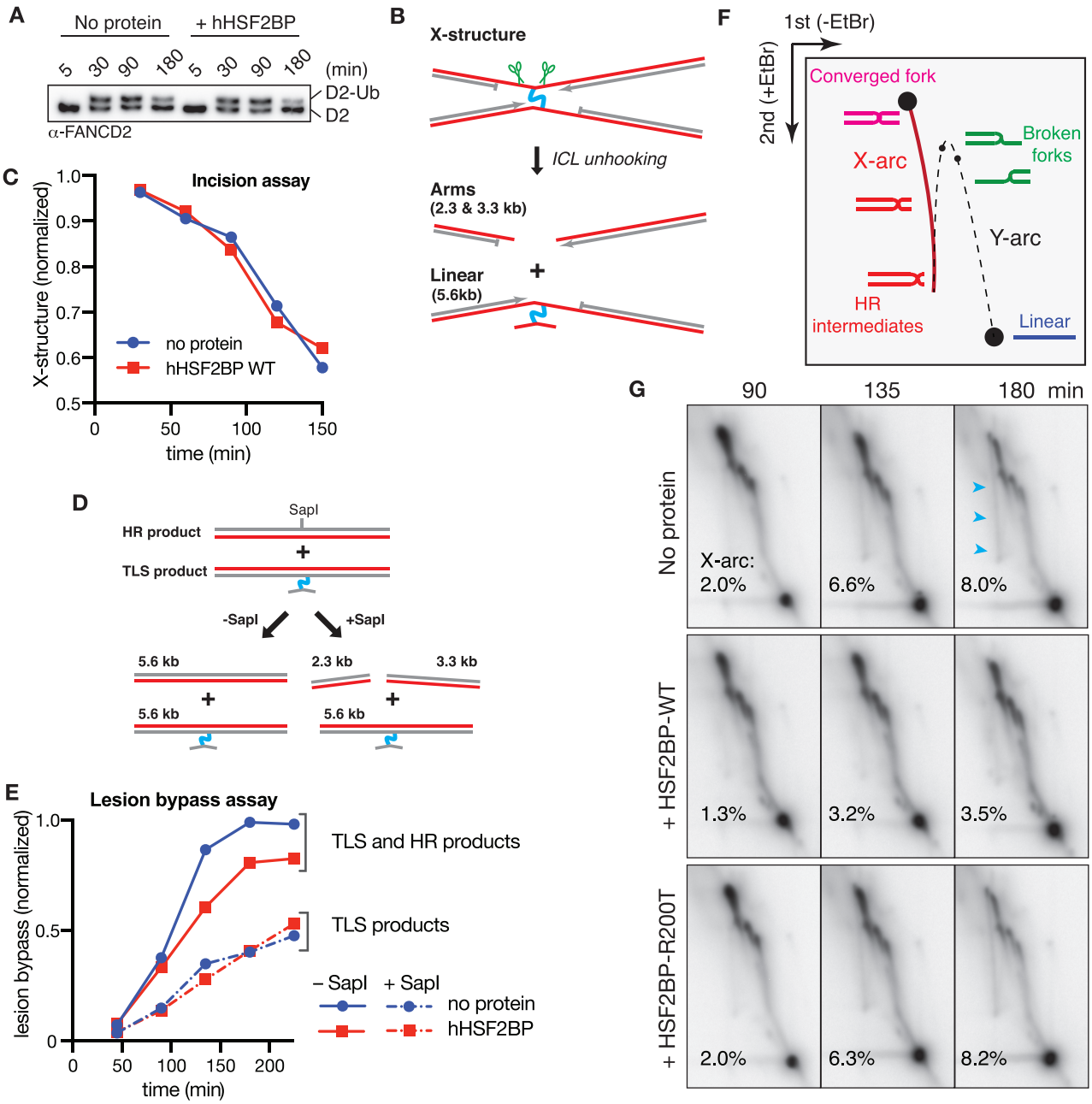

Figure 3. HSF2BP inhibits HR in the FA pathway. (**A**) HSF2BP does not inhibit ICL-induced FANCD2 ubiquitination in *Xenopus* egg extract. Proteins from egg extract incubated with pICL with or without the addition of recombinant human HSF2BP for the indicated periods of time were analyzed by immunoblotting with anti-*Xenopus laevis* FANCD2 antibody. (**B** and **C**) HSF2BP does not inhibit lesion unhooking in *Xenopus* egg extract. Prelabeled pICL was replicated in *Xenopus* egg extracts supplemented with or without recombinant human HSF2BP, and replication products were isolated, digested by HincII to generate the products shown on the scheme (B), and separated on a denaturing agarose gel (Supplementary Figure S3C). The decline of the X-structures was quantified and plotted (C). Red lines on the scheme (B) indicate the labeled parental strand. (**D** and **E**) HSF2BP does not inhibit translesion synthesis in *Xenopus* egg extract. pICL was replicated in *Xenopus* egg extracts supplemented with or without recombinant human HSF2BP in the presence of ^{32}P-α-dCTP, and replication products were isolated, digested by HincII, or HincII and SapI, as shown on the scheme (D), and separated on a denaturing agarose gel (Supplementary Figure S3D). Extension products were quantified and plotted (E). HSF2BP-induced reduction in full-length products in the absence of SapI indicates a defect in HR. (**F** and **G**) Inhibition of HR intermediate formation by HSF2BP revealed by 2DGE. pICL was replicated in *Xenopus* egg extracts supplemented with or without recombinant human HSF2BP in the presence of ^{32}P-α-dCTP, and replication products were isolated, digested by HincII, and analyzed by 2DGE. Scheme (F) shows migration patterns for various replication products. The X-arc is indicated by the blue arrows in the top right image in (G), the numbers indicate the efficiency of its formation (defined by the ratio of X-arc product intensity to total intensity).

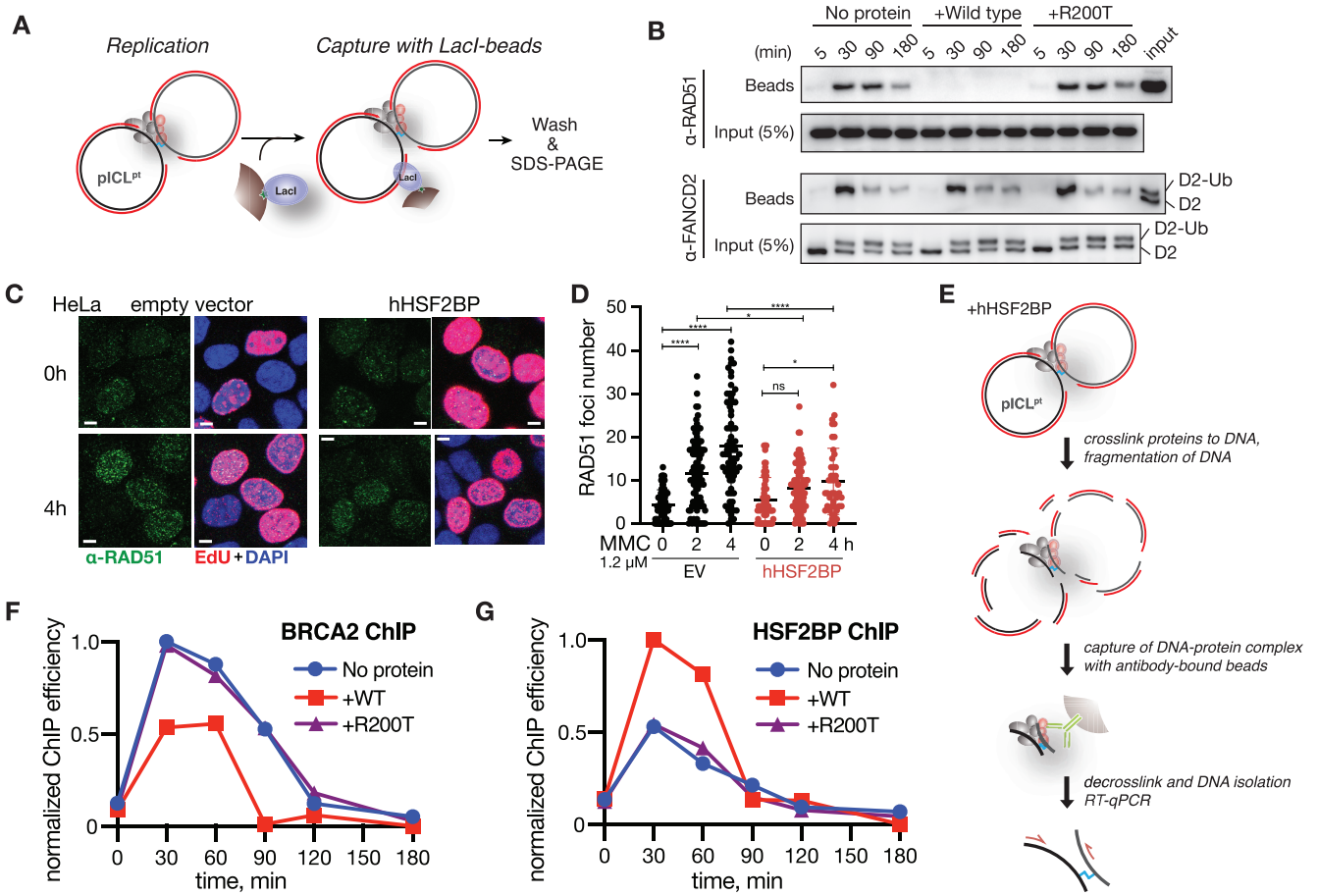

Figure 4. HSF2BP–BRCA2 interaction prevents RAD51 accumulation at ICL. (**A** and **B**) Stable RAD51 accumulation on pICL during repair is abrogated by wild-type human HSF2BP, but not the R200T mutant. The pICL plasmid was replicated in *Xenopus* egg extracts. At the indicated times, pICL was pulled down by incubation with streptavidin beads coated with biotinylated LacI (A). Presence of bound RAD51 and FANCD2 was determined by immunoblotting (B). (**C** and **D**) RAD51 focus formation after short-term (0–4 h) exposure to 1.2 μM MMC of HeLa cells stably transformed with human HSF2BP expression vector or an empty vector. Thirty minutes before fixation, EdU was added to the media to label S-phase cells. After Click-IT reaction and anti-RAD51 immunofluorescent staining, cells were imaged using confocal microscope. Representative images (C) and foci quantification (D) are shown. Foci were counted manually. The experiment was repeated two times, 50–90 nuclei per sample were analyzed, significance was determined using one-way ANOVA; scale bars = 5 μm. Experiment with chronic MMC treatment is shown in Supplementary Figure S4A. (**E**) Scheme of the ChIP assay. (**F** and **G**) Recombinant human HSF2BP inhibits loading of endogenous BRCA2 at the ICL in *Xenopus* egg extract. pICL replication samples at the indicated time points were analyzed by BRCA2 (F) and HSF2BP (G) ChIP using a primer pair for the ICL locus.

TLS polymerase REV1 and FANCD2 to the ICL was not affected in the presence of HSF2BP (Supplementary Figure S4B–D), further establishing that HSF2BP inhibits ICL repair downstream of the FA pathway activation, ICL incision and TLS.

HSF2BP induces ICL repair-dependent unloading and degradation of BRCA2

To gain mechanistic understanding of how BRCA2–HSF2BP interaction prevents RAD51 loading, we monitored the levels of BRCA2 during ICL repair in *Xenopus* egg extract. Strikingly, in the presence of wild-type HSF2BP, but not the R200T mutant, BRCA2 was progressively degraded during repair (Figure 5A). Addition of the proteasome inhibitor MG-132, in combination with recombinant ubiquitin to prevent ubiquitin depletion, fully blocked BRCA2 degradation during ICL repair indicating that the degradation is proteasome-mediated (Figure 5B). The degradation was ICL-dependent, as it was not induced when a non-damaged control plasmid was replicated in the presence of hHSF2BP (Figure 5C). In addition, the degradation is initiated upstream of nucleolytic incisions that unhook the ICL, because blocking these incisions by immunodepletion of XPF-ERCC1 still resulted in BRCA2 degradation (Supplementary Figure S5A). To examine whether the reduced levels of BRCA2 at the ICL in the presence of hHSF2BP (Figure 4F) are directly caused by BRCA2 degradation, we performed ChIP on repair intermediates generated in the presence of MG-132. Surprisingly, even though BRCA2 is not degraded under these conditions, its presence at the ICL is still reduced to the same extent compared to the condition without proteasomal inhibition (Figure 5D and Supplementary Figure S5B). Consistent with this, proteasomal inhibition did not rescue the HSF2BP-induced ICL repair defect (Figure 5E and Supplementary Figure S5C).

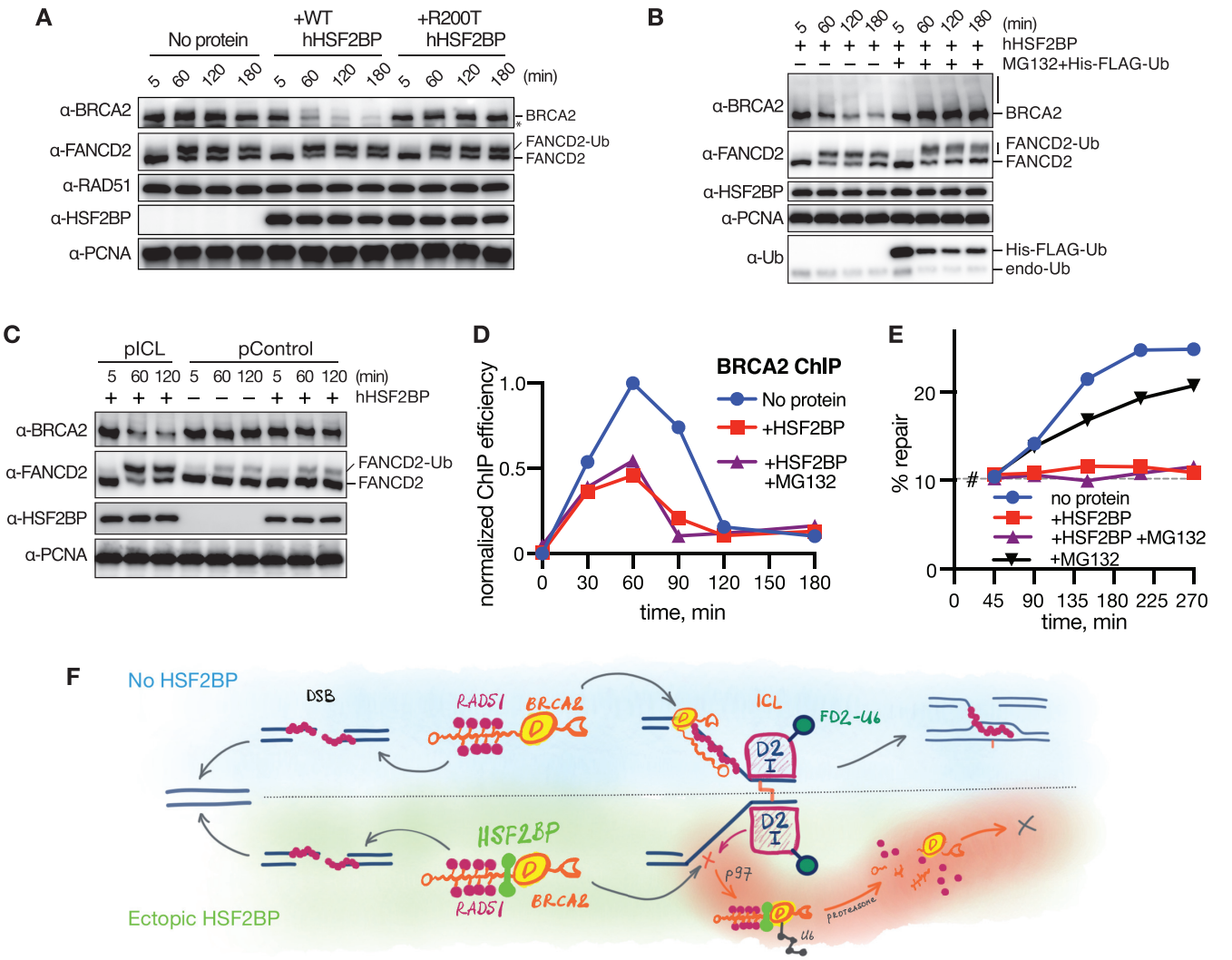

Figure 5. HSF2BP induces ICL-dependent BRCA2 degradation. (**A**) Wild-type HSF2BP, but not the R200T mutant, induces BRCA2 degradation during ICL repair. pICL was replicated in *Xenopus* egg extracts in the presence or absence of human HSF2BP. Total extract samples were collected at the indicated time points and analyzed by immunoblotting. (**B**) HSF2BP-induced BRCA2 degradation is proteasome dependent. pICL was replicated in *Xenopus* egg extracts containing human HSF2BP in the absence or presence of proteasome inhibitor MG-132. Recombinant His-FLAG-tagged ubiquitin was added to counteract ubiquitin depletion as a result of proteasome inhibition. Total extract samples were collected at the indicated time points and analyzed by immunoblotting. (**C**) HSF2BP-induced BRCA2 degradation is ICL repair-dependent. Experiment as in (A) was repeated with the pControl plasmid that has the same sequence as pICL, but no crosslink. Total extract samples were collected at the indicated time points and analyzed by immunoblotting. (**D**) Addition of MG-132 does rescue reduced level of BRCA2 at ICLs during repair. Crosslinked plasmids were replicated in the presence or absence of purified recombinant wild-type human HSF2BP, with and without MG-132 and His-FLAG-tagged ubiquitin. Samples were analyzed by BRCA2 ChIP using a primer pair for the ICL locus. (**E**) HSF2BP-induced ICL repair defect is not rescued upon addition of MG-132. ICL repair efficiency in *Xenopus* egg extract was measured in the presence or absence of purified recombinant wild-type human HSF2BP with and without MG-132 and His-FLAG-tagged ubiquitin. #, SapI fragments from contaminating uncrosslinked plasmid present in varying amounts in different pICL preparations. (**F**) Schematic depiction of the model explaining HSF2BP effects on the function of BRCA2 in DSB and ICL repair.

These findings indicate that the repair defect is caused by the HSF2BP-mediated removal of BRCA2 from the ICL and that BRCA2 degradation by the proteasome is a downstream event. Ubiquitin-mediated extraction of proteins from the chromatin is often mediated by the p97 segregase (62) and allows subsequent proteasomal degradation. Consistent with a similar model, we detected potential ubiquitin chains on BRCA2 upon proteasome inhibition (Figure 5B), and addition of a p97 inhibitor prevented HSF2BP-induced BRCA2 degradation (Supplementary Figure S5D). Taken together, we propose that HSF2BP promotes BRCA2 ubiquitination at ICL sites that leads to its p97-dependent extraction from the chromatin, preventing stable RAD51 accumulation at the ICL, leading to inhibition of HR.

DISCUSSION

Our findings detail the molecular mechanism by which ectopic production of a meiotic HR protein HSF2BP negatively affects ICL repair in somatic tumor-derived cells.

They provide experimental evidence in support of the appealing but not extensively tested hypothesis that meiotic DNA metabolism, when induced out of context, could induce transformation-promoting genomic instability. Ectopic expression of germline genes has been previously shown to either increase (23,28–29,63–66) or decrease (21–22,25,27,30) the resistance of cancer cells to DNA damage. While both effects can promote tumor development, genome destabilization is expected to be more relevant in the initial stages of carcinogenic transformation. Importantly, we find that HSF2BP amplification is mutually exclusive with pathological BRCA2 mutations, suggesting it could drive tumorigenesis by inducing genome instability.

While HSF2BP promotes HR during meiosis (3,4), we describe how it suppresses HR during ICL repair in somatic cancer cells. This apparent contradiction is not surprising taking into account the major differences between mitotic and meiotic DNA transactions. For example, while in mitotic cells BRCA2 functions to chaperone only the RAD51 strand exchange protein, during meiosis it needs to orchestrate homologous recombination activities between both RAD51 and DMC1. Given the proximity of the HSF2BP binding domain (2270–2337) to the two DMC1-binding sites in BRCA2: the region containing the PhePP motif (2386–2411) (67) and the BRC repeats 6–8 (68) (1837–2085), it is possible that the HSF2BP–BRCA2 interaction is required for the formation of the combined RAD51-DMC1 nucleoprotein filament at meiotic DSBs, but creates a degradation-inducing BRCA2 conformation when DMC1 is absent during the ICL repair in mitosis. However, as the substitution of phenylalanine 2406, a residue reported to be essential for DMC1 binding *in vitro* (67), with aspartic acid had no effect on fertility in mice (69), and the role of BRC6–8 in meiosis has not been tested *in vivo*, the relevance of the proximity is unclear.

The effect of HSF2BP on BRCA2 in cancer cells is highly specific as it manifests only in the context of PARPi resistance and ICL repair by the FA pathway, effectively creating a separation of function condition for BRCA2. This observation has several important implications. First, we believe this is more consistent with the putative role in transformation, as it emerges that gradual or segmental losses of BRCA2 function are more conducive to tumorigenesis (70–72) compared to the catastrophic consequences of its complete inactivation, which generally leads to cell death. The interplay between *HSF2BP* activity and the production of *BRCA2* Δ12 splice form could provide additional plasticity in modulating BRCA2 function. Second, it creates a vulnerability that can be targeted by specific therapies, as exemplified by the acute sensitivity of HSF2BP-producing cells to PARPi. Third, the ability to experimentally isolate BRCA2 function in ICL repair from its other roles provides a tool for further mechanistic understanding of this complex essential protein. This could be of similar importance as the previous identification of mutations that specifically affect BRCA2′s role in replication fork stabilization (73,74).

The similarity of the cellular phenotype induced by HSF2BP to that of FA patient cells raises an interesting possibility that FA-like genomic instability syndromes may not require any mutations affecting protein sequences. Although this is a well-established concept in molecular oncology (proto-oncogene activation) and there are examples of genetic diseases and developmental abnormalities caused by ectopic gene expression in humans and in model organisms (75–78), ectopic activation of wild-type genes is outside of the current FA diagnostic paradigm. The same applies to genetic analysis of HR-deficient tumors, which generally does not take HR attenuators into account as a possible cause. Therefore, the identification and monitoring of these ectopically expressed genes could facilitate diagnosis and allow better treatment options.

Our findings also open up a new way to study the origin of PARPi sensitivity in FA cells, which currently not well understood. Interestingly, sensitization to PARPi by ectopic HSF2BP production is closer to the levels observed in cells deficient in FA core (79–82) compared to cells deficient in HR proteins (BRCA2, PALB2, RAD51, BRCA1), which are much more sensitive. This indicates that BRCA2 contributes to PARPi resistance via multiple pathways, some of which also may also involve the FA core proteins. The phenotype of HSF2BP-producing cells also suggests that response to ionizing radiation is not a universal predictor of cancer cell 'BRCAness', as they are not sensitive to the irradiation, but are sensitive to PARPi and ICL-inducing agents.

Biochemical recapitulation of ICL repair in *Xenopus* egg extracts revealed no effect on the initial steps of repair (FA pathway activation, ICL unhooking and TLS), but defective HR due to ICL repair-dependent removal of BRCA2 from the lesion followed by BRCA2 degradation preventing stable RAD51 loading. This, together with our previous finding that BRCA2 and HSF2BP are in a constitutive complex, leads us to the following model (Figure 5F). During ICL repair, the HSF2BP–BRCA2 complex is efficiently recruited to the ICL, where the presence of HSF2BP causes local BRCA2 ubiquitination and removal of the protein from the lesion site by the p97 segregase. Once removed from the chromatin, BRCA2 is efficiently degraded by the proteasome. In the absence of the mediator function of BRCA2, RAD51 nucleoprotein filaments cannot be stably formed at the lesion, leading to the failure of downstream HR steps that depend on homology search and strand exchange. Although it is currently not clear what triggers HSF2BP-mediated BRCA2 ubiquitination, we show that its degradation does not depend on the generation of the DSB by XPF-ERCC1-dependent unhooking. This indicates that ubiquitination and BRCA2 unloading are initiated upstream during ICL repair. Since BRCA2 is known to be recruited to and stabilize stalled replication forks (73,74), we speculate that the recruitment and degradation could be coupled, possibly by an HSF2BP-mediated interaction with a stalled fork-associated ubiquitin E3 ligase. Although this model is speculative, it would explain why HSF2BP does not compromise those forms of BRCA2-dependent HR that are not preceded by a stalled replication fork, and why HSF2BP-producing cells are sensitive to PARPi.

Further investigation of the meiotic defect caused by HSF2BP loss and ICL repair suppression by its ectopic production should provide exciting details about BRCA2 roles in HR, allow to better reconcile the seemingly disparate functions of HSF2BP, establish the molecular details of FA-

HR engagement and advance the understanding of the genetic underpinnings of FA and cancer.

SUPPLEMENTARY DATA

Supplementary Data are available at NAR Online.

ACKNOWLEDGEMENTS

Author contributions: A.Z. and R.K. conceived the study. I.B., A.Z., N.V. and A.O. performed human cell and biochemical experiments. K.S. performed *Xenopus* egg extract experiments. K.S. and S.Ev.R.F. purified the proteins. J.C.D., D.vG., P.K., A.Z. and R.K. supervised different parts of the study. A.Z., P.K., R.K. and K.S. wrote the manuscript with contributions from other authors. All authors read and approved the manuscript.

FUNDING

Uehara Memorial Foundation (to K.S.); Mochida Memorial Foundation for Medical and Pharmaceutical Research (to K.S.); JSPS Postdoctoral Fellowship for Research Abroad (to K.S.); Netherlands Organization for Scientific Research (NWO) [VIDI 700.10.421 to P.K. and Gravitation Program CancerGenomiCs.nl]; Dutch Cancer Society [KWF HUBR 2015-7736, EMCR 2008-4045, Ride for the Roses Cancer Research Grant]; European Community's Seventh Framework Program [FP7/2007-2013, HEALTH-F2-2010-259893]. This research is part of the Oncode Institute, which is partly financed by the Dutch Cancer Society. Funding for open access charge: Dutch Cancer Society.
Conflict of interest statement. None declared.

REFERENCES

1. Prakash,R., Zhang,Y., Feng,W. and Jasin,M. (2015) Homologous recombination and human health: the roles of BRCA1, BRCA2, and associated proteins. *Cold Spring Harb. Perspect. Biol.*, **7**, a016600.
2. Zhang,F., Ma,J., Wu,J., Ye,L., Cai,H., Xia,B. and Yu,X. (2009) PALB2 links BRCA1 and BRCA2 in the DNA-damage response. *Curr. Biol.*, **19**, 524–529.
3. Brandsma,I., Sato,K., van Rossum-Fikkert,S.E., van Vliet,N., Sleddens,E., Reuter,M., Odijk,H., van den Tempel,N., Dekkers,D.H.W., Bezstarosti,K. *et al.* (2019) HSF2BP Interacts with a conserved domain of BRCA2 and is required for mouse spermatogenesis. *Cell Rep.*, **27**, 3790–3798.
4. Zhang,J., Fujiwara,Y., Yamamoto,S. and Shibuya,H. (2019) A meiosis-specific BRCA2 binding protein recruits recombinases to DNA double-strand breaks to ensure homologous recombination. *Nat. Commun.*, **10**, 722.
5. Yoshima,T., Yura,T. and Yanagi,H. (1998) Novel testis-specific protein that interacts with heat shock factor 2. *Gene*, **214**, 139–146.
6. Zelensky,A.N., Kanaar,R. and Wyman,C. (2014) Mediators of Homologous DNA Pairing. *Cold Spring Harb. Perspect. Biol.*, **6**, a016451–a016451.
7. Lord,C.J., Tutt,A.N.J. and Ashworth,A. (2015) Synthetic lethality and cancer therapy: lessons learned from the development of PARP inhibitors. *Annu. Rev. Med.*, **66**, 455–470.
8. Kottemann,M.C. and Smogorzewska,A. (2013) Fanconi anaemia and the repair of Watson and Crick DNA crosslinks. *Nature*, **493**, 356–363.
9. Auerbach,A.D. (2009) Fanconi anemia and its diagnosis. *Mutat. Res.*, **668**, 4–10.
10. Klein Douwel,D., Boonen,R.A.C.M., Long,D.T., Szypowska,A.A., Räschle,M., Walter,J.C. and Knipscheer,P. (2014) XPF-ERCC1 acts in Unhooking DNA interstrand crosslinks in cooperation with FANCD2 and FANCP/SLX4. *Mol. Cell*, **54**, 460–471.
11. Long,D.T., Raschle,M., Joukov,V. and Walter,J.C. (2011) Mechanism of RAD51-Dependent DNA interstrand Cross-Link Repair. *Science*, **333**, 84–87.
12. Donoho,G., Brenneman,M.A., Cui,T.X., Donoviel,D., Vogel,H., Goodwin,E.H., Chen,D.J. and Hasty,P. (2003) Deletion of Brca2 exon 27 causes hypersensitivity to DNA crosslinks, chromosomal instability, and reduced life span in mice. *Genes Chromosomes Cancer*, **36**, 317–331.
13. Meijer,T.G., Verkaik,N.S., Sieuwerts,A.M., van Riet,J., Naipal,K.A.T., van Deurzen,C.H.M., Bakker den,M.A., Sleddens,H.F.B.M., Dubbink,H.-J., Toom den,T.D. *et al.* (2018) Functional ex vivo assay reveals homologous recombination deficiency in breast cancer beyond BRCA gene defects. *Clin. Cancer Res.*, **24**, 6277–6287.
14. Lord,C.J. and Ashworth,A. (2016) BRCAness revisited. *Nat. Rev. Cancer*, **16**, 110–120.
15. Bruggeman,J.W., Koster,J., Lodder,P., Repping,S. and Hamer,G. (2018) Massive expression of germ cell-specific genes is a hallmark of cancer and a potential target for novel treatment development. *Oncogene*, **37**, 5694–5700.
16. Gibbs,Z.A. and Whitehurst,A.W. (2018) Emerging contributions of Cancer/Testis antigens to neoplastic behaviors. *Trends Cancer*, **4**, 701–712.
17. McFarlane,R.J. and Wakeman,J.A. (2017) Meiosis-like functions in oncogenesis: A new view of cancer. *Cancer Res.*, **77**, 5712–5716.
18. Simpson,A.J.G., Caballero,O.L., Jungbluth,A., Chen,Y.-T. and Old,L.J. (2005) Cancer/testis antigens, gametogenesis and cancer. *Nat. Rev. Cancer*, **5**, 615–625.
19. Wang,C., Gu,Y., Zhang,K., Xie,K., Zhu,M., Dai,N., Jiang,Y., Guo,X., Liu,M., Dai,J. *et al.* (2016) Systematic identification of genes with a cancer-testis expression pattern in 19 cancer types. *Nat. Commun.*, **7**, 10499.
20. Almeida,L.G., Sakabe,N.J., deOliveira,A.R., Silva,M.C.C., Mundstein,A.S., Cohen,T., Chen,Y.-T., Chua,R., Gurung,S., Gnjatic,S. *et al.* (2009) CTdatabase: a knowledge-base of high-throughput and curated data on cancer-testis antigens. *Nucleic Acids Res.*, **37**, D816–D819.
21. Nielsen,A.Y. and Gjerstorff,M.F. (2016) Ectopic expression of testis germ cell proteins in cancer and its potential role in genomic instability. *Int. J. Mol. Sci.*, **17**, E890.
22. Lindsey,S.F., Byrnes,D.M., Eller,M.S., Rosa,A.M., Dabas,N., Escandon,J. and Grichnik,J.M. (2013) Potential role of meiosis proteins in melanoma chromosomal instability. *J Skin Cancer*, **2013**, 190109.
23. Gao,Y., Mutter-Rottmayer,E., Greenwalt,A.M., Goldfarb,D., Yan,F., Yang,Y., Martinez-Chacin,R.C., Pearce,K.H., Tateishi,S., Major,M.B. *et al.* (2016) A neomorphic cancer cell-specific role of MAGE-A4 in trans-lesion synthesis. *Nat. Commun.*, **7**, 12105.
24. Hosoya,N., Okajima,M., Kinomura,A., Fujii,Y., Hiyama,T., Sun,J., Tashiro,S. and Miyagawa,K. (2011) Synaptonemal complex protein SYCP3 impairs mitotic recombination by interfering with BRCA2. *EMBO Rep.*, **13**, 44–51.
25. Greve,K.B.V., Lindgreen,J.N., Terp,M.G., Pedersen,C.B., Schmidt,S., Mollenhauer,J., Kristensen,S.B., Andersen,R.S., Relster,M.M., Ditzel,H.J. *et al.* (2015) Ectopic expression of cancer/testis antigen SSX2 induces DNA damage and promotes genomic instability. *Mol. Oncol.*, **9**, 437–449.
26. Shiohama,Y., Ohtake,J., Ohkuri,T., Noguchi,D., Togashi,Y., Kitamura,H. and Nishimura,T. (2014) Identification of a meiosis-specific protein, MEIOB, as a novel cancer/testis antigen and its augmented expression in demethylated cancer cells. *Immunol. Lett.*, **158**, 175–182.
27. Khan,J., Ezan,F., Crémet,J.-Y., Fautrel,A., Gilot,D., Lambert,M., Benaud,C., Troadec,M.-B. and Prigent,C. (2011) Overexpression of active Aurora-C kinase results in cell transformation and tumour formation. *PLoS One*, **6**, e26512.
28. Gao,Y., Kardos,J., Yang,Y., Tamir,T.Y., Mutter-Rottmayer,E., Weissman,B., Major,M.B., Kim,W.Y. and Vaziri,C. (2018) The Cancer/Testes (CT) Antigen HORMAD1 promotes homologous recombinational DNA Repair and radioresistance in lung adenocarcinoma cells. *Sci. Rep.*, **8**, 15304.
29. Wang,X., Tan,Y., Cao,X., Kim,J.A., Chen,T., Hu,Y., Wexler,M. and Wang,X. (2018) Epigenetic activation of HORMAD1 in basal-like

breast cancer: role in Rucaparib sensitivity. *Oncotarget*, **9**, 30115–30127.
30. Watkins,J., Weekes,D., Shah,V., Gazinska,P., Joshi,S., Sidhu,B., Gillett,C., Pinder,S., Vanoli,F., Jasin,M. *et al.* (2015) Genomic complexity profiling reveals that HORMAD1 overexpression contributes to homologous recombination deficiency in Triple-Negative breast cancers. *Cancer Discov.*, **5**, 488–505.
31. Cadinanos,J. and Bradley,A. (2007) Generation of an inducible and optimized piggyBac transposon system. *Nucleic Acids Res.*, **35**, e87.
32. Yusa,K., Zhou,L., Li,M.A., Bradley,A. and Craig,N.L. (2011) A hyperactive piggyBac transposase for mammalian applications. *Proc. Natl. Acad. Sci. U.S.A.*, **108**, 1531–1536.
33. Ran,F.A., Hsu,P.D., Wright,J., Agarwala,V., Scott,D.A. and Zhang,F. (2013) Genome engineering using the CRISPR-Cas9 system. *Nat. Protoc.*, **8**, 2281–2308.
34. Zelensky,A.N., Schimmel,J., Kool,H., Kanaar,R. and Tijsterman,M. (2017) Inactivation of Pol θ and C-NHEJ eliminates off-target integration of exogenous DNA. *Nat. Commun.*, **8**, 66.
35. Gibson,D.G., Young,L., Chuang,R.-Y., Venter,J.C., Hutchison,C.A. and Smith,H.O. (2009) Enzymatic assembly of DNA molecules up to several hundred kilobases. *Nat. Meth.*, **6**, 343–345.
36. Geissmann,Q. (2013) OpenCFU, a new free and open-source software to count cell colonies and other circular objects. *PLoS One*, **8**, e54072.
37. Puget,N., Knowlton,M. and Scully,R. (2005) Molecular analysis of sister chromatid recombination in mammalian cells. *DNA Repair (Amst.)*, **4**, 149–161.
38. Zelensky,A.N., Sanchez,H., Ristic,D., Vidic,I., van Rossum-Fikkert,S.E., Essers,J., Wyman,C. and Kanaar,R. (2013) Caffeine suppresses homologous recombination through interference with RAD51-mediated joint molecule formation. *Nucleic Acids Res.*, **41**, 6475–6489.
39. Tan,T.L., Essers,J., Citterio,E., Swagemakers,S.M., de Wit,J., Benson,F.E., Hoeijmakers,J.H. and Kanaar,R. (1999) Mouse Rad54 affects DNA conformation and DNA-damage-induced Rad51 foci formation. *Curr. Biol.*, **9**, 325–328.
40. Chalkley,G.E. and Verrijzer,C.P. (2004) Immuno-depletion and purification strategies to study chromatin-remodeling factors in vitro. *Meth. Enzymol.*, **377**, 421–442.
41. Budzowska,M., Graham,T.G.W., Sobeck,A., Waga,S. and Walter,J.C. (2015) Regulation of the Rev1-pol ζ complex during bypass of a DNA interstrand cross-link. *EMBO J.*, **34**, 1971–1985.
42. Kochaniak,A.B., Habuchi,S., Loparo,J.J., Chang,D.J., Cimprich,K.A., Walter,J.C. and van Oijen,A.M. (2009) Proliferating cell nuclear antigen uses two distinct modes to move along DNA. *J. Biol. Chem.*, **284**, 17700–17710.
43. Räschle,M., Knipscheer,P., Knipsheer,P., Enoiu,M., Angelov,T., Sun,J., Griffith,J.D., Ellenberger,T.E., Schärer,O.D. and Walter,J.C. (2008) Mechanism of replication-coupled DNA interstrand crosslink repair. *Cell*, **134**, 969–980.
44. Walter,J. and Newport,J. (2000) Initiation of eukaryotic DNA replication: origin unwinding and sequential chromatin association of Cdc45, RPA, and DNA polymerase alpha. *Mol. Cell*, **5**, 617–627.
45. Rodrigue,A., Lafrance,M., Gauthier,M.-C., McDonald,D., Hendzel,M., West,S.C., Jasin,M. and Masson,J.-Y. (2006) Interplay between human DNA repair proteins at a unique double-strand break in vivo. *EMBO J.*, **25**, 222–231.
46. Walter,J., Sun,L. and Newport,J. (1998) Regulated chromosomal DNA replication in the absence of a nucleus. *Mol. Cell*, **1**, 519–529.
47. Tutter,A.V. and Walter,J.C. (2006) Chromosomal DNA replication in a soluble cell-free system derived from Xenopus eggs. *Methods Mol. Biol.*, **322**, 121–137.
48. Enoiu,M., Ho,T.V., Long,D.T., Walter,J.C. and Schärer,O.D. (2012) Construction of plasmids containing site-specific DNA interstrand cross-links for biochemical and cell biological studies. *Methods Mol. Biol.*, **920**, 203–219.
49. Knipscheer,P., Räschle,M., Schärer,O.D. and Walter,J.C. (2012) Replication-coupled DNA interstrand cross-link repair in Xenopus egg extracts. *Methods Mol. Biol.*, **920**, 221–243.
50. Modesti,M., Budzowska,M., Baldeyron,C., Demmers,J.A.A., Ghirlando,R. and Kanaar,R. (2007) RAD51AP1 is a structure-specific DNA binding protein that stimulates joint molecule formation during RAD51-mediated homologous recombination. *Mol. Cell*, **28**, 468–481.
51. Klein Douwel,D., Hoogenboom,W.S., Boonen,R.A. and Knipscheer,P. (2017) Recruitment and positioning determine the specific role of the XPF-ERCC1 endonuclease in interstrand crosslink repair. *EMBO J.*, **36**, 2034–2046.
52. Pacek,M., Tutter,A.V., Kubota,Y., Takisawa,H. and Walter,J.C. (2006) Localization of MCM2-7, Cdc45, and GINS to the site of DNA unwinding during eukaryotic DNA replication. *Mol. Cell*, **21**, 581–587.
53. Gao,J., Aksoy,B.A., Dogrusoz,U., Dresdner,G., Gross,B., Sumer,S.O., Sun,Y., Jacobsen,A., Sinha,R., Larsson,E. *et al.* (2013) Integrative analysis of complex cancer genomics and clinical profiles using the cBioPortal. *Sci. Signal.*, **6**, pl1.
54. Cerami,E., Gao,J., Dogrusoz,U., Gross,B.E., Sumer,S.O., Aksoy,B.A., Jacobsen,A., Byrne,C.J., Heuer,M.L., Larsson,E. *et al.* (2012) The cBio cancer genomics portal: an open platform for exploring multidimensional cancer genomics data. *Cancer Discov.*, **2**, 401–404.
55. Knipscheer,P., Räschle,M., Smogorzewska,A., Enoiu,M., Ho,T.V., Schärer,O.D., Elledge,S.J. and Walter,J.C. (2009) The Fanconi anemia pathway promotes replication-dependent DNA interstrand cross-link repair. *Science*, **326**, 1698–1701.
56. Fackenthal,J.D., Yoshimatsu,T., Zhang,B., de Garibay,G.R., Colombo,M., De Vecchi,G., Ayoub,S.C., Lal,K., Olopade,O.I., Vega,A. *et al.* (2016) Naturally occurring BRCA2 alternative mRNA splicing events in clinically relevant samples. *J. Med. Genet.*, **53**, 548–558.
57. Li,L., Biswas,K., Habib,L.A., Kuznetsov,S.G., Hamel,N., Kirchhoff,T., Wong,N., Armel,S., Chong,G., Narod,S.A. *et al.* (2009) Functional redundancy of exon 12 of BRCA2 revealed by a comprehensive analysis of the c.6853A>G (p.I2285V) variant. *Hum. Mutat.*, **30**, 1543–1550.
58. Rauh-Adelmann,C., Lau,K.M., Sabeti,N., Long,J.P., Mok,S.C. and Ho,S.M. (2000) Altered expression of BRCA1, BRCA2, and a newly identified BRCA2 exon 12 deletion variant in malignant human ovarian, prostate, and breast cancer cell lines. *Mol. Carcinog.*, **28**, 236–246.
59. Bièche,I. and Lidereau,R. (1999) Increased level of exon 12 alternatively spliced BRCA2 transcripts in tumor breast tissue compared with normal tissue. *Cancer Res.*, **59**, 2546–2550.
60. Garcia-Higuera,I., Taniguchi,T., Ganesan,S., Meyn,M.S., Timmers,C., Hejna,J., Grompe,M. and D'Andrea,A.D. (2001) Interaction of the Fanconi anemia proteins and BRCA1 in a common pathway. *Mol. Cell*, **7**, 249–262.
61. Long,D.T., Joukov,V., Budzowska,M. and Walter,J.C. (2014) BRCA1 promotes unloading of the CMG helicase from a stalled DNA replication fork. *Mol. Cell*, **56**, 174–185.
62. Franz,A., Ackermann,L. and Hoppe,T. (2016) Ring of Change: CDC48/p97 drives protein dynamics at chromatin. *Front. Genet.*, **7**, 73.
63. Nichols,B.A., Oswald,N.W., McMillan,E.A., McGlynn,K., Yan,J., Kim,M.S., Saha,J., Mallipeddi,P.L., LaDuke,S.A., Villalobos,P.A. *et al.* (2018) HORMAD1 Is a Negative Prognostic Indicator in Lung Adenocarcinoma and Specifies Resistance to Oxidative and Genotoxic Stress. *Cancer Res.*, **78**, 6196–6208.
64. Cappell,K.M., Sinnott,R., Taus,P., Maxfield,K., Scarbrough,M. and Whitehurst,A.W. (2012) Multiple cancer testis antigens function to support tumor cell mitotic fidelity. *Mol. Cell. Biol.*, **32**, 4131–4140.
65. Whitehurst,A.W., Xie,Y., Purinton,S.C., Cappell,K.M., Swanik,J.T., Larson,B., Girard,L., Schorge,J.O. and White,M.A. (2010) Tumor antigen acrosin binding protein normalizes mitotic spindle function to promote cancer cell proliferation. *Cancer Res.*, **70**, 7652–7661.
66. Shahzad,M.M.K., Shin,Y.-H., Matsuo,K., Lu,C., Nishimura,M., Shen,D.-Y., Kang,Y., Hu,W., Mora,E.M., Rodriguez-Aguayo,C. *et al.* (2013) Biological significance of HORMA domain containing protein 1 (HORMAD1) in epithelial ovarian carcinoma. *Cancer Lett.*, **330**, 123–129.
67. Thorslund,T., Esashi,F. and West,S.C. (2007) Interactions between human BRCA2 protein and the meiosis-specific recombinase DMC1. *EMBO J.*, **26**, 2915–2922.
68. Martinez,J.S., von Nicolai,C., Kim,T., Ehlen,A., Mazin,A.V., Kowalczykowski,S.C. and Carreira,A. (2016) BRCA2 regulates DMC1-mediated recombination through the BRC repeats. *Proc. Natl Acad. Sci. U.S.A.*, **113**, 3515–3520.

69. Biswas,K., Das,R., Eggington,J.M., Qiao,H., North,S.L., Stauffer,S., Burkett,S.S., Martin,B.K., Southon,E., Sizemore,S.C. *et al.* (2012) Functional evaluation of BRCA2 variants mapping to the PALB2-binding and C-terminal DNA-binding domains using a mouse ES cell-based assay. *Hum. Mol. Genet.*, **21**, 3993–4006.
70. Feng,W. and Jasin,M. (2018) Homologous recombination and replication fork protection: BRCA2 and More! *Cold Spring Harb. Symp. Quant. Biol.*, **82**, 329–338.
71. Hartford,S.A., Chittela,R., Ding,X., Vyas,A., Martin,B., Burkett,S., Haines,D.C., Southon,E., Tessarollo,L. and Sharan,S.K. (2016) Interaction with PALB2 is essential for maintenance of genomic integrity by BRCA2. *PLos Genet.*, **12**, e1006236.
72. Tan,S.L.W., Chadha,S., Liu,Y., Gabasova,E., Perera,D., Ahmed,K., Constantinou,S., Renaudin,X., Lee,M., Aebersold,R. *et al.* (2017) A class of environmental and endogenous toxins induces brca2 haploinsufficiency and genome instability. *Cell*, **169**, 1105–1118.
73. Lomonosov,M., Anand,S., Sangrithi,M., Davies,R. and Venkitaraman,A.R. (2003) Stabilization of stalled DNA replication forks by the BRCA2 breast cancer susceptibility protein. *Genes Dev.*, **17**, 3017–3022.
74. Schlacher,K., Christ,N., Siaud,N., Egashira,A., Wu,H. and Jasin,M. (2011) Double-strand break repair-independent role for BRCA2 in blocking stalled replication fork degradation by MRE11. *Cell*, **145**, 529–542.
75. Lee,T.I. and Young,R.A. (2013) Transcriptional regulation and its misregulation in disease. *Cell*, **152**, 1237–1251.
76. Prelich,G. (2012) Gene overexpression: uses, mechanisms, and interpretation. *Genetics*, **190**, 841–854.
77. Epstein,D.J. (2009) Cis-regulatory mutations in human disease. *Brief. Funct. Genomic. Proteomic.*, **8**, 310–316.
78. Jaenisch,R. and Bird,A. (2003) Epigenetic regulation of gene expression: how the genome integrates intrinsic and environmental signals. *Nat. Genet.*, **33**, 245–254.
79. Lombardi,A.J., Hoskins,E.E., Foglesong,G.D., Wikenheiser-Brokamp,K.A., Wiesmüller,L., Hanenberg,H., Andreassen,P.R., Jacobs,A.J., Olson,S.B., Keeble,W.W. *et al.* (2015) Acquisition of relative interstrand crosslinker resistance and PARP inhibitor sensitivity in fanconi anemia head and neck cancers. *Clin. Cancer Res.*, **21**, 1962–1972.
80. McCabe,N., Turner,N.C., Lord,C.J., Kluzek,K., Bialkowska,A., Swift,S., Giavara,S., O'Connor,M.J., Tutt,A.N., Zdzienicka,M.Z. *et al.* (2006) Deficiency in the repair of DNA damage by homologous recombination and sensitivity to poly(ADP-ribose) polymerase inhibition. *Cancer Res.*, **66**, 8109–8115.
81. Murai,J., Huang,S.-Y.N., Das,B.B., Renaud,A., Zhang,Y., Doroshow,J.H., Ji,J., Takeda,S. and Pommier,Y. (2012) Trapping of PARP1 and PARP2 by Clinical PARP Inhibitors. *Cancer Res.*, **72**, 5588–5599.
82. Stoepker,C., Faramarz,A., Rooimans,M.A., van Mil,S.E., Balk,J.A., Velleuer,E., Ameziane,N., Riele,Te, H. and de Winter,J.P. (2015) DNA helicases FANCM and DDX11 are determinants of PARP inhibitor sensitivity. *DNA Repair (Amst.)*, **26**, 54–64.